nature portfolio

Peer Review File

Dimensional Control of Low-Dimensional Perovskite Hybrids for Photovoltaics

Corresponding Author: Professor Hao Chen

Parts of this Peer Review File have been redacted as indicated to remove third-party material.

This file contains all reviewer reports in order by version, followed by all author rebuttals in order by version.

Version 0:

Reviewer comments:

Reviewer #1

(Remarks to the Author)
The authors develop a series of bis-imidazolium ligands to precisely control the formation of low-dimensional perovskites, establishing clear structure-property relationships between ligand design and resulting perovskite dimensionality. Distinct from conventional studies, this work begins with the design of organic ligands, establishing an in-depth relationship between the chemical structure of the ligands and the dimensionality and architecture of the induced single crystals. In addition, the study provided a detailed and comprehensive structural analysis of both the ligands and the single crystals, and achieved a high efficiency in the final device, demonstrating a certified efficiency of over 27% and exceptional stability. Overall, this study is of great importance and may attract broad interest in the related fields. The experimental results are solid and convincing. Therefore, I would recommend publication in Nature Communications after the authors adequately address the following comments:
1. The device performance and analysis of chemical and structural properties with low-dimensional perovskites were well provided. But still, the reason for choosing the specific organic ligands is unclear. Why were bis-imidazolium ligands chosen, and what advantages do they offer compared to monofunctional imidazolium ligands? The author may need to strengthen the rationale explanation.
2. The authors first optimized the intrinsic molecular structures of the four ligands. What is the primary purpose of highlighting this part of the study?
3. Further detailed elucidation is necessary to explain the differences in performance enhancement of perovskite devices resulting from the distinct one-dimensional perovskite structures induced by Dim-C2-CN and Dim-C4-CN.
4. In the device section, it is necessary to supplement the statistical photovoltaic parameters of devices incorporating different concentrations of Dim-C4-CN.
5. On the defect properties, the authors provided PL mapping results, yet no related discussion was given. Further providing the PLQY results and QFLS analysis would strengthen the discussion on the defect properties and performance improvements of related devices. In addition, detailed information on the optical characterizations, e.g. TRPL and PL mapping, needs to be provided.
6. There are some typos, including the reference formats and some figure labels, need to be checked and corrected.

Reviewer #2

(Remarks to the Author)
This study presents a molecular design strategy for bis-imidazolium ligands that enables precise dimensional control over perovskite architectures, ranging from 0D to parallel and bridged 1D configurations. By systematically varying terminal functional groups and inter-imidazolium spacing, author achieved controlled crystallization of high-quality 1D-3D hybrid perovskite films with optimized crystallization kinetics and charge transport properties. Consequently, photovoltaic devices fabricated using these materials yield a certified PCE of 27.02%—representing a record performance for dimensionally engineered perovskite solar cells. This study provides universal design principles for perovskite dimensional modulation at the molecular level, holding significant theoretical and applied value for advancing the development of high-efficiency and stable perovskite optoelectronic devices. This study, both in its mechanistic investigations and experimental analyses — particularly regarding perovskite single crystals and ligand structural design — strikes me as an exceptionally sound and

meaningful piece of research. Therefore, I recommend the acceptance of this study following the implementation of the minor revisions outlined below.
1. Please elaborate on the reasons for selecting this specific series of ligands in the research design. The rationale for employing -CN as terminal modifications in the ligand design requires further explanation. Furthermore, apart from the -CN polar group, it is suggested that the author provide further clarification on whether other similar polar groups exhibit the same phenomenon.
2. XRD patterns of the organic salts should be provided to compare with their perovskites or perovskite/perovskite heterostructures.
3. Will the formation of 1d-3d hybrid perovskites affect the hydrophobicity of the film? It is recommended to provide contact Angle data.
4. Does the formation of low-dimensional perovskite change the residual strain in 3D perovskite films? It is suggested that the author provide evidence to illustrate. Please reference: https://doi.org/10.1002/aenm.202101018.
5. The author should further prove "Upon increasing the concentration of the three ligands, well-defined low-dimensional perovskite phases were preferentially accumulating at 3D perovskite grain boundaries" through experimental data.
6. The positions of the Pb 4f7/2 and Pb 4f5/2 peaks in Fig. S30 are incorrect. It is recommended that the author correct them.
7. It is suggested that the authors standardize the format of the nuclear magnetic resonance hydrogen spectra of the molecules in Figures S1-S8; it is recommended that the format of the relative energy values of molecules in Figures S9-S12 be unified.
8. “mofidied” in the caption of Fig. 2 should be “modified”, and the spelling needs to be proofread.

Reviewer #3

(Remarks to the Author)
In this work, the authors successfully synthesized and characterized four distinct perovskite single-crystal structures by systematically modulating organic ligand chemistry. These crystals were effectively integrated into perovskite photovoltaic devices, achieving a certified power conversion efficiency (PCE) exceeding 27% along with excellent operational stability. The study demonstrates significant innovation, particularly in establishing explicit structure-property relationships between organic ligand design and low-dimensional crystal architectures. Supported by comprehensive characterization, I believe this work will significantly advance future research on low-dimensional/three-dimensional (2D/3D) heterojunction systems. Therefore, I would recommend this manuscript for publication in Nature Communications after the following revisions are addressed.
Comments to the authors：
1.Regarding the single-crystal structures induced by the Dim-C2-CN and Dim-C4-CN ligands, does the current study focus exclusively on cyano (-CN) modified systems? It would be helpful to know if the investigation was extended to explore the specific crystal structures induced by ligands functionalized with other types of substituents, or if the -CN group was specifically chosen for a particular chemical reason.
2.When substituting a methyl group with a cyano group on the ligand, it is necessary to elucidate the specific advantages conferred by this modification, either in terms of the ligand’s own properties or the resulting single-crystal packing. Please provide a clearer rationale for the selection of CN-functionalized ligands in this study.
3.The origin of the simplified structural representation in Figure 1c should be clarified. Please specify whether it was obtained through computational simulation (e.g., DFT) or if it is a schematic abstraction of an experimentally determined single-crystal structure.
4.For the stability tests conducted under 85°C and 85% relative humidity (ISOS-D-3), the authors should present the actual efficiency evolution data (absolute PCE values) in the supplement, rather than reporting only the normalized efficiency values.
5.It was observed that the optimal concentrations of the added ligands differ between the 1.54 eV and wide-bandgap (WBG) devices. To better understand these system-dependent effects, the impact of varying ligand concentrations on device performance should be systematically discussed across the different bandgap regimes.
6.There appears to be an inaccuracy in the caption of Figure 2. The authors should carefully verify and correct the descriptions to ensure they match the data shown.

Version 1:

Reviewer comments:

Reviewer #1

(Remarks to the Author)
The authors have performed additional characterizations on the structural and defect properties of the different perovskites, which have properly addressed my previous concerns. I would recommend acceptance of the revised manuscript in Nature Communications.

Reviewer #2

(Remarks to the Author)
The authors have adequately responded to all my comments and revised the manuscript appropriately. The revised version meets the publication standard of the journal, and I recommend acceptance.

Reviewer #3

(Remarks to the Author)
The authors have addressed my concerns. I would recommend publishing this work in its current form.

Point-by-point actions in response to the Reviewers' comments

We thank the reviewers for their advice and recommendations, which have enabled us to improve our manuscript. Following are the detailed actions taken in light of reviewers' comments.

Reviewer #1:

The authors develop a series of bis-imidazolium ligands to precisely control the formation of low-dimensional perovskites, establishing clear structure-property relationships between ligand design and resulting perovskite dimensionality. Distinct from conventional studies, this work begins with the design of organic ligands, establishing an in-depth relationship between the chemical structure of the ligands and the dimensionality and architecture of the induced single crystals. In addition, the study provided a detailed and comprehensive structural analysis of both the ligands and the single crystals, and achieved a high efficiency in the final device, demonstrating a certified efficiency of over 27% and exceptional stability. Overall, this study is of great importance and may attract broad interest in the related fields. The experimental results are solid and convincing. Therefore, I would recommend publication in Nature Communications after the authors adequately address the following comments:

Response: We thank the reviewer for the positive comments.

1. The device performance and analysis of chemical and structural properties with low-dimensional perovskites were well provided. But still, the reason for choosing the specific organic ligands is unclear. Why were bis-imidazolium ligands chosen, and what advantages do they offer compared to monofunctional imidazolium ligands? The author may need to strengthen the rationale explanation.

Response: We thank the reviewer for raising this valuable question. Our previous work focused on low-dimensional perovskites induced by mono-imidazolium ligands (*Adv. Mater.* 2024, 36, 2401476 and *Adv. Energy Mater.* 2024, 14, 2400021). Through single-crystal structural analysis, we observed that mono-imidazolium ligands coordinate to PbI_2 units via a single imidazolium ring. Building on this insight, in the present study

we designed and report a novel bis-imidazolium ligand structure. Compared with the previously reported mono-imidazolium ligands, the bis-imidazolium ligand possesses a greater number of binding sites for lead iodide, which confers two principal advantages. First, the additional binding units function as a molecular bridge, enabling both ends of the ligand to connect with the PbI_3^- one dimensional chains, thereby forming a more stable and robust bridging architecture-as exemplified by the bridged one-dimensional perovskite structure induced by the Dim-C4-CN ligand elucidated in this work. Second, the bis-imidazolium ligand can provide two electron-rich imidazolium rings/nitrogen atoms, allowing simultaneous passivation of two defect sites at the perovskite surface or grain boundaries. This "bidentate" passivation effect is more thorough and robust than the "monodentate" passivation offered by mono-functional ligands, leading to a more effective reduction in the density of non-radiative recombination centers.

After finalizing the bis-imidazolium ligand framework, we tuned the end groups of the ligand's chemical structure and adjusted the length of the terminal units to better match the periodicity of the lead iodide units. Furthermore, by extending the carbon chain between the two imidazolium rings, we optimized the inter-imidazolium distance. These structural modifications ultimately enabled the formation of a stable, bridged one-dimensional perovskite architecture.

2. The authors first optimized the intrinsic molecular structures of the four ligands. What is the primary purpose of highlighting this part of the study?

Response: We thank the reviewer for raising this valuable question. Since all four ligands share a common bis-imidazolium core and possess terminal functional groups, each ligand can theoretically adopt four distinct conformations, as illustrated in Figures S9-S12. The distance between the imidazolium rings and the effective length of the terminal groups differ significantly across these conformations. Given that our study reveals that both the inter-imidazolium distance and the length of the terminal groups play a decisive role in determining the structure of the resulting low-dimensional perovskite, we first performed detailed conformational optimization of each ligand in

DMSO. This computational approach was undertaken to identify the most probable chemical structure for each ligand, thereby enabling the measurement of key parameters such as the inter-imidazolium distance and the terminal group length. Based on these parameters, we were then able to predict the type of low-dimensional structure each ligand is likely to induce.

Action: (In Page 4)

We designed four modulated dual-imidazolium ligands (Dim-C2-CH_3, Dim-C2-OMe, Dim-C2-CN and Dim-C4-CN) to explore the correlation between ligand structures and the dimensionality of novel low-dimensional perovskite phases (Fig. 1a and Supplementary Figs. S1-S8). To investigate the energetically favorable configurations of the dual-imidazolium ligands in DMSO, density functional theory (DFT) calculations were conducted (Supplementary Figs. S9-S12). Comparative analysis of their lowest-energy configurations revealed that polar groups reduce the terminal distance due to electrostatic attraction to the imidazole rings (CH_3: 5.90 > OMe: 4.96 Å > CN: 4.09 Å), while increasing the carbon spacer between the imidazole rings extends the inter-imidazolium distance (Fig. 1b). In particular, Dim-C2-CH_3, Dim-C2-OMe, and Dim-C2-CN exhibit inter-imidazolium distances of 4.70 Å, 4.78 Å, and 4.76 Å respectively, closely matching the 4.05 Å periodicity of $[PbI_3]^-$ motifs. Dim-C4-CN has an extended inter-imidazolium distance (8.79 Å), capable to bridge two $[PbI_3]^-$motifs.

3. Further detailed elucidation is necessary to explain the differences in performance enhancement of perovskite devices resulting from the distinct one-dimensional perovskite structures induced by Dim-C2-CN and Dim-C4-CN.

Response: We thank the reviewer for raising this insightful question. The Dim-C4-CN ligand can more effectively modulate the perovskite crystallization process, which originates from its stronger interaction with the perovskite components. This stronger interaction results in a perovskite film with more uniform morphology and higher crystallinity. Furthermore, the low-dimensional perovskite induced by Dim-C4-CN exhibits more pronounced orientation, which is more favorable for charge transport.

Additionally, the enhanced effectiveness of the Dim-C4-CN ligand in promoting charge transport was corroborated by electrochemical impedance spectroscopy, dark current measurements, and Mott-Schottky analysis.

Action: (In page 7)

XRD analysis of Dim-C4-CN confirmed the presence of the 1D perovskite phase Dim-C4-CN$(PbI_3)_2$, with peak positions and relative intensities matching precisely with single-crystal reference data (Supplementary Fig. S37). All three low-dimensional/3D perovskite films exhibit significantly enhanced 3D perovskite peak intensities, compared to the reference film, demonstrating that the low-dimensional modification strategy substantially improves bulk crystallinity (Fig. 3e). Notably, the Dim-C4-CN-modified perovskite demonstrates superior crystallinity among the samples, corroborating the morphological observations. GIWAXS analysis further indicates that the 1D perovskite phase derived from Dim-C4-CN exhibits a markedly enhanced out-of-plane orientation within the 3D perovskite matrix compared to its Dim-C2-CN counterpart (Fig. 3f). Such preferential orientation is anticipated to facilitate more efficient vertical charge transport, thereby contributing to the overall improvement in device performance.

4. In the device section, it is necessary to supplement the statistical photovoltaic parameters of devices incorporating different concentrations of Dim-C4-CN.

Response: We thank the reviewer for the valuable suggestion. An analysis of the impact of different concentrations of Dim-C4-CN on the photovoltaic parameters of the device has been supplemented accordingly.

Action: (In the supporting information)

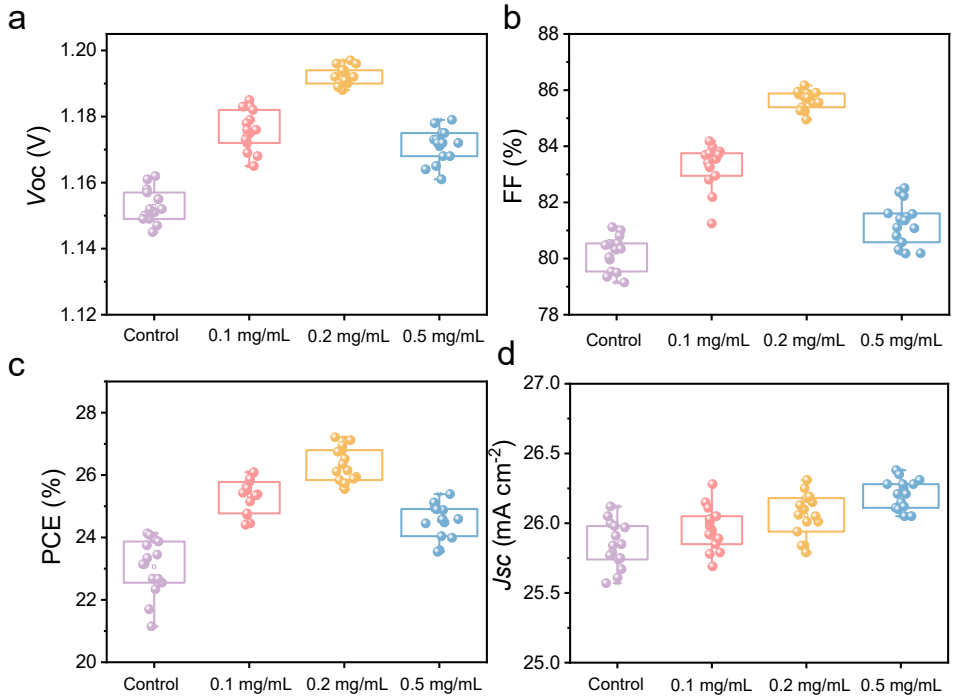

Fig. S40. Photovoltaic performance statistics of the devices with bandgaps of 1.54 eV treated with varying concentrations of Dim-C4-CN. The statistics of photovoltaic performance parameters of control and ligands-modified PSCs: (a) *V*oc, (b) FF, (c) PCE and (d) *J*sc.

Action: (In page 8)

The devices were fabricated with a conventional inverted structure, exhibiting a bandgap of 1.54 eV. The reference device achieved a PCE of 24.13%, while the Dim-C2-CH_3 and Dim-C2-CN-modified devices demonstrated improved PCEs of 25.46% and 25.17%, respectively. Notably, the champion device based on Dim-C4-CN modification achieved a superior PCE of 27.21% with a *V*oc of 1.197 V, a *J*sc of 26.37 mA/cm^2 and a FF of 86.21% (Supplementary Fig. S39-40 and Supplementary Tables S32-33), demonstrating the most significant performance enhancement among all modified devices. The cross-sectional SEM images of the device are also provided in Supplementary Fig. S41. The J_{SC} values derived from current density-voltage (*J*-*V*) measurements show excellent agreement with the integrated external quantum efficiency (EQE) spectra (Supplementary Fig. S42).

5. On the defect properties, the authors provided PL mapping results, yet no related discussion was given. Further providing the PLQY results and QFLS analysis would strengthen the discussion on the defect properties and performance improvements of related devices. In addition, detailed information on the optical characterizations, e.g. TRPL and PL mapping, needs to be provided.

Response: We would like to express our sincere gratitude to the reviewers for their valuable suggestions. In response, we have supplemented the discussion on the PL mapping results to elucidate the specific impact of low-dimensional perovskite modifications on their three-dimensional counterparts. Furthermore, supplementary details regarding the specific optical measurement configurations are provided.

To strengthen the analysis of defect properties and the associated device performance enhancements, we carried out additional photoluminescence quantum yield (PLQY) measurements and performed a quantitative analysis of the corresponding quasi-Fermi level splitting (QFLS). The PLQY of both control and ligand-modified perovskite films were measured, and the corresponding QFLS values were derived (Figure R1). The control perovskite film exhibits a PLQY value of 7.510%, corresponding to a QFLS of 1.185 eV. In comparison, the Dim-C4-CN-modified sample achieves a maximum PLQY of 12.82%, corresponding to an elevated QFLS value of 1.200 eV.

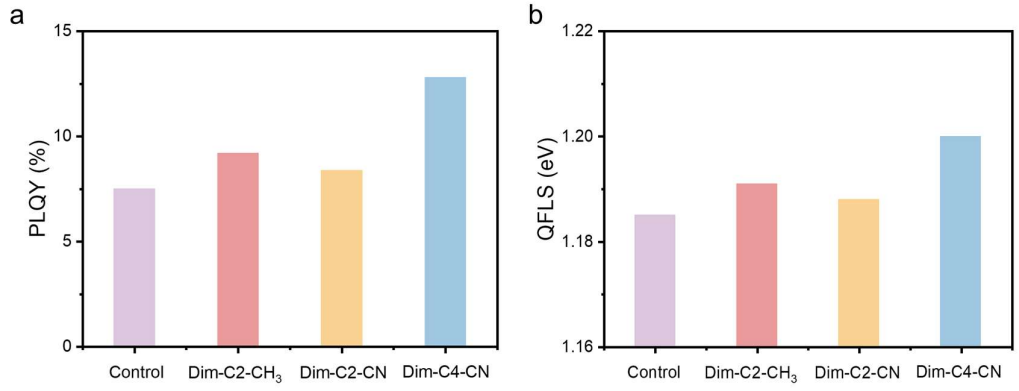

Figure R1. (a) PLQY values and (b) QFLS values for perovskite films.

Action: (In page 6)

To fundamentally understand the chemical passivation mechanism enabled by this low-dimensional modification approach, we conducted comprehensive photoluminescence

(PL) studies including spatial mapping (Fig. 2d) (Supplementary Fig. S33). Compared to the reference, all three ligand-modified perovskite films exhibit enhanced PL intensity, with the Dim-C4-CN-modified perovskite film showing the strongest PL signal. Time-resolved photoluminescence (TRPL) further reveal that the Dim-C4-CN-modified perovskite films exhibit prolonged charge-carrier lifetimes, which we attribute to the effective suppression of non-radiative recombination via trap-state passivation[32–34]. The reduction in defect state density achieved through low-dimensional perovskite formation was further confirmed by space-charge-limited current (SCLC) measurements[35,36] (Supplementary Figs. S34-35), providing additional quantitative confirmation of the improved electronic quality in modified films.

Action: (In the supporting information)

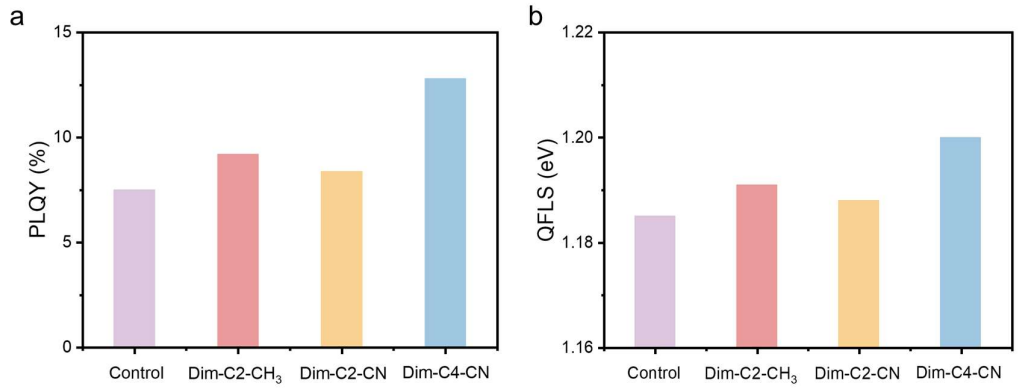

Fig. S49. (a) PLQY values and (b) QFLS values for perovskite films.

Action: (In page 9)

The performance enhancement can be attributed to optimized charge transport dynamics and effective suppression of non-radiative recombination, as corroborated by electrochemical impedance spectroscopy (EIS) and conventional Mott-Schottky measurements (Supplementary Figs. S47-48). To further substantiate the analysis of the concomitant enhancement in device performance, we conducted additional photoluminescence quantum yield (PLQY) measurements and quantitatively evaluated the corresponding quasi-Fermi level splitting (QFLS). The PLQY of both the control and ligand-modified perovskite films were acquired, from which the respective QFLS values were derived (Figure S49). The control perovskite film exhibits a PLQY of

7.510%, translating to a QFLS of 1.185 eV. In contrast, the Dim-C4-CN-modified film attains a markedly improved PLQY of 12.82%, corresponding to an elevated QFLS of 1.200 eV. The spatially confined photogenerated carriers in 0D perovskites system[47] and the poor orientation of parallel-aligned 1D perovskites system, fundamentally limit further enhancement of charge transport properties.

Action: (In page 20)

XRD patterns were obtained by Rigaku Smart Lab (λ= 1.54 Å). The single crystal X-ray diffraction data of $(Dim\text{-}C2\text{-}CH_3)_3Pb_3I_{4.9}Br_{7.1}$, $Dim\text{-}C2\text{-}OMe(PbI_3)_2$, $Dim\text{-}C2\text{-}CN(PbI_3)_2$ and $Dim\text{-}C4\text{-}CN(PbI_3)_2$ were collected at 299 K using Cu radiation (λ = 1.54178 Å) on a Bruker SMART APEX II CCD detector. The relevant crystallographic results can be found in Table S2. Time-resolved photoluminescence (TRPL) measurements were performed using an FLS 1000 fluorescence spectrometer (Edinburgh Instruments, UK) equipped with a 445 nm laser. Steady-state photoluminescence (PL) mapping measurements were performed u a Meite Optoelectronics system at a scan rate of 1 Hz to ensure high image quality. The excitation source was a continuous-wave diode laser with a wavelength of 445 nm, focused onto the sample surface through a 100× objective lens. The PL emission was collected by the same objective and directed to a spectrometer equipped with a charge-coupled device (CCD) detector. The mapping area was 50 × 50 μm². All measurements were conducted under ambient conditions at room temperature. Atomic force microscopy (AFM) and Kelvin probe force microscopy (KPFM) images were collected at a Bruker AFM. Topographic images of the films were captured using a Bruker AFM equipped with a Dimension Edge and ScanAsyst in tapping mode.

6. There are some typos, including the reference formats and some figure labels, need to be checked and corrected.

Response: We thank the reviewer for the careful review. A thorough re-examination and revision of the entire manuscript has been conducted accordingly.

Action: (In page 23)

Fig. 2. Characterization of perovskite films. (**a**) AFM and (**c**) KPFM images of control, Dim-C2-CH_3, Dim-C2-CN and Dim-C4-CN-mofidied perovskite films. (**c**) Statistical analysis of potential distribution. (**d**) PL mapping of control, Dim-C2-CH_3, Dim-C2-CN and Dim-C4-CN-mofidied perovskite films.

Action: (In page 13)

40. Li, S. *et al.* Anion-Cation Synergistic Regulation of Low-Dimensional Perovskite Passivation Layer for Perovskite Solar Cells. *Adv. Mater.* **37**, 2500988 (2025).

Reviewer #2:

This study presents a molecular design strategy for bis-imidazolium ligands that enables precise dimensional control over perovskite architectures, ranging from 0D to parallel and bridged 1D configurations. By systematically varying terminal functional groups and inter-imidazolium spacing, author achieved controlled crystallization of high-quality 1D-3D hybrid perovskite films with optimized crystallization kinetics and charge transport properties. Consequently, photovoltaic devices fabricated using these materials yield a certified PCE of 27.02%—representing a record performance for dimensionally engineered perovskite solar cells. This study provides universal design principles for perovskite dimensional modulation at the molecular level, holding significant theoretical and applied value for advancing the development of high-efficiency and stable perovskite optoelectronic devices. This study, both in its mechanistic investigations and experimental analyses — particularly regarding perovskite single crystals and ligand structural design — strikes me as an exceptionally sound and meaningful piece of research. Therefore, I recommend the acceptance of this study following the implementation of the minor revisions outlined below.

Response: We thank the reviewer for the positive comments.

1. Please elaborate on the reasons for selecting this specific series of ligands in the research design. The rationale for employing -CN as terminal modifications in the ligand design requires further explanation. Furthermore, apart from the -CN polar group,

it is suggested that the author provide further clarification on whether other similar polar groups exhibit the same phenomenon.

Response: The cyano group, owing to its high polarity and strong coordination ability, can form coordination interactions with lead ions (Pb^{2+}) in perovskite precursors. This interaction modulates the crystallization kinetics, thereby facilitating the formation of dense and morphologically uniform thin films. Additionally, the cyano group effectively suppresses ion migration within the perovskite lattice and achieves efficient defect passivation through bonding with defect sites (Nature 2024, 628, 306–312; *Nat. Mater.* 2025, 24, 770–777 and *Angew. Chem. Int. Ed.* 2025, 64, e202504902). In our study, in-situ grazing-incidence wide-angle X-ray scattering (GIWAXS) and in-situ absorption measurements were employed to confirm the effective role of the cyano-containing ligand Dim-C4-CN in modulating the crystallization process of perovskite. Analysis of the GIWAXS patterns further revealed that Dim-C4-CN promotes the formation of a perovskite film with high crystallinity.

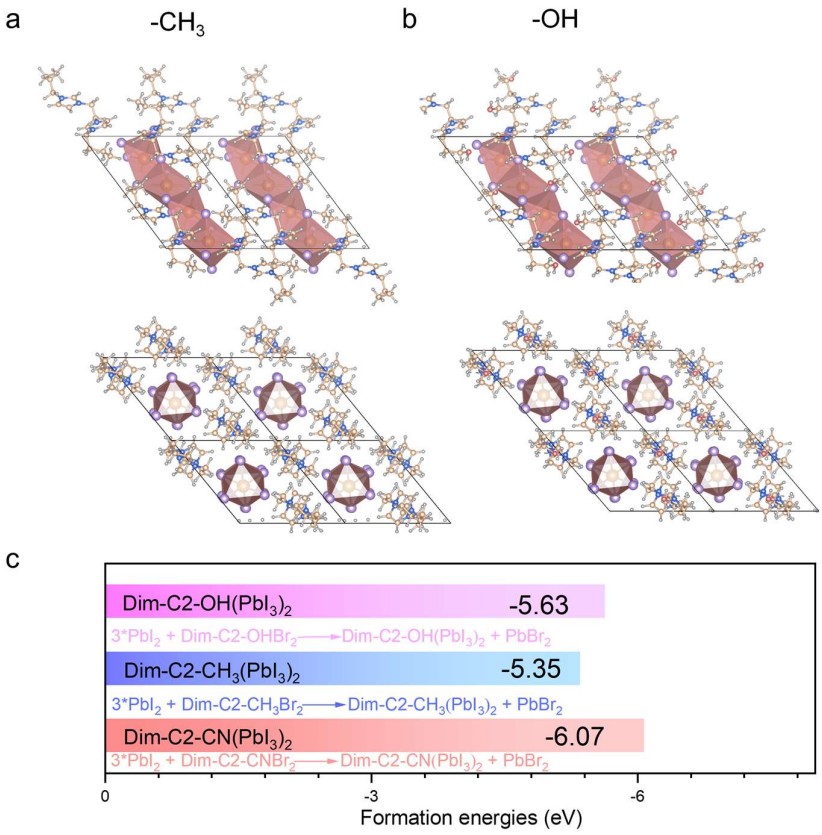

Figure R2. Side (first row) and top view (second row) of the DFT optimized crystal structures of (a) Dim-C2-$CH_3(PbI_3)_2$ and (b) Dim-C_2-$OH(PbI_3)_2$. (c) Formation energies of the Dim-C2-$CH_3(PbI_3)_2$, Dim-C2-$CH_3(PbI_3)_2$, and Dim-C2-$CH_3(PbI_3)_2$ crystals computed by DFT calculations.

For the single-crystal structure induced by the Dim-C2-CN ligand (Figure R2), DFT calculations revealed that replacing the -CN group with -CH_3 or -OH leads to formation energies of -5.35 eV and -5.63 eV, respectively, which are lower than that of the cyano-containing system. Similarly, in the analysis of the single-crystal structure induced by Dim-C4-CN (Figure R3), DFT calculations showed that substituting the -CN group with -CH_3 (-6.28 eV) or -OH (-6.43 eV) also reduces the crystal formation energy compared to that of the -CN system (-6.71 eV).

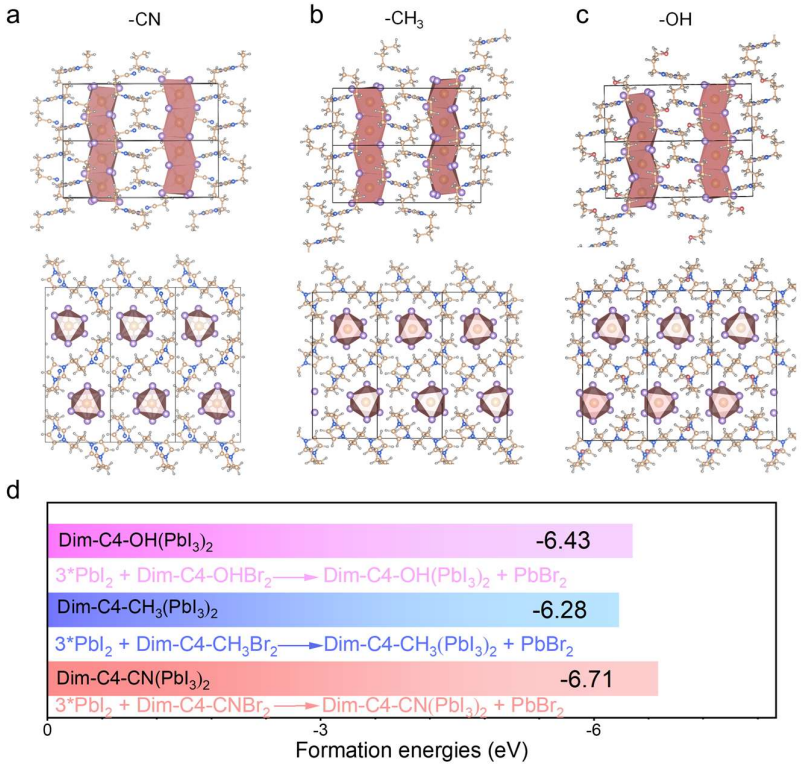

Figure R3. (a-c) Simulation of the single crystal structure 1D Dim-C4-$CN(PbI_3)_2$ after replacing the -CN in the ligand Dim-C4-CN with a -CH_3 or -OH group. Formation energies of the Dim-C4-$CH_3(PbI_3)_2$, (Dim-C4-$CH_3(PbI_3)_2$, and Dim-C4-$CH_3(PbI_3)_2$ crystals computed by DFT calculations.

Action: (In page 5)

The ligands with methoxy groups (Dim-C2-OMe) and cyano groups (Dim-C2-CN) both yield a 1D perovskite crystal Dim-C2-$OMe(PbI_3)_2$ (Supplementary Tables S9-16) and Dim-C2-$CN(PbI_3)_2$ (Supplementary Tables S17-24), where the terminal distances

reduced to 4.90 and 4.06 Å (Fig. 1c), respectively in line with the DFT results. Moreover, the DFT calculations show an isostructural 1D perovskite crystal when replacing the CN groups with OH groups (Supplementary Figs. S17-18) and the CN groups (-6.07 eV) showed larger crystal formation energy than the CH_3 (-5.35 eV) and OH (-5.63 eV) groups.

Action: (In page 5)

Extending inter-imidazolium chain length from Dim-C2-CN scaffold to Dim-C4-CN transformed the parallel 1D orientation to a bridged 1D architecture (Fig. 1d), Dim-C4-CN$(PbI_3)_2$, which is classified within the monoclinic crystal (space group P 21/c. Supplementary Tables S25-31). This configuration enhances interchain connectivity via ligand-mediated bridging, markedly stabilizing the perovskite framework. DFT calculations show that further substitution of CN groups (-6.71 eV) with CH_3 (-6.28 eV) or -OH (-6.43 eV) groups reduced the crystal formation energy(Supplementary Figs. S19-20). The formation energy of Dim-C4-CN $(PbI_3)_2$ (-6.71 eV) is lower than that of Dim-C2-CN $(PbI_3)_2$ (-6.07 eV), indicating stronger thermodynamic stability of the Dim-C4-CN-induced 1D perovskite structure.

2. XRD patterns of the organic salts should be provided to compare with their perovskites or perovskite/perovskite heterostructures.

Response: The authors gratefully acknowledge the reviewers for their valuable suggestions. In response, we have supplemented the XRD patterns of the four organic ligands and provided them in the Supporting Information. In comparison with the XRD patterns of ligand-induced low-dimensional perovskite single crystals, no characteristic diffraction peaks corresponding to the respective ligands were observed in the low-dimensional perovskite single crystals.

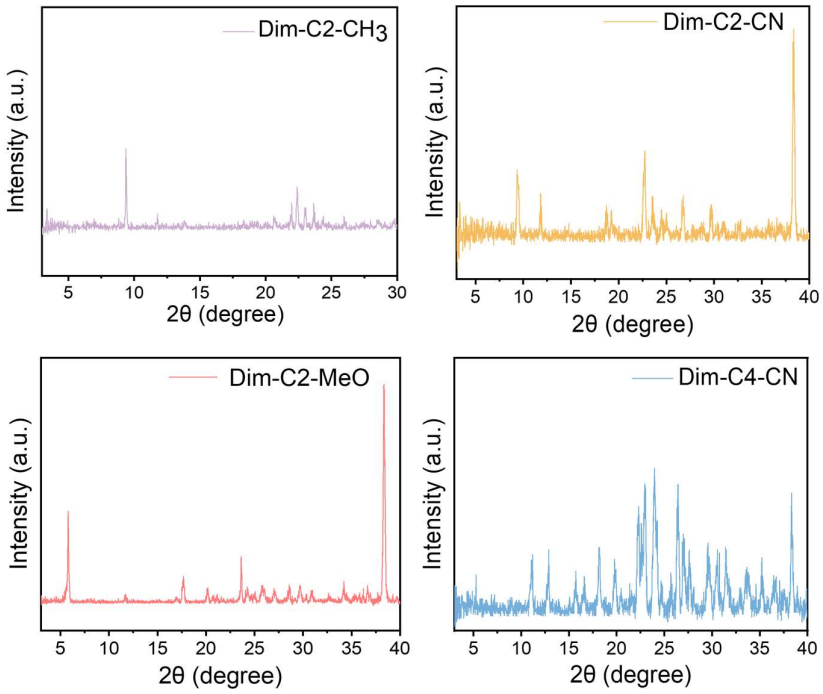

Figure R3. XRD patterns of organic ligands: Dim-C2-CH_3, Dim-C2-CN, Dim-C2-MeO and Dim-C4-CN.

Action: (In the supporting information)

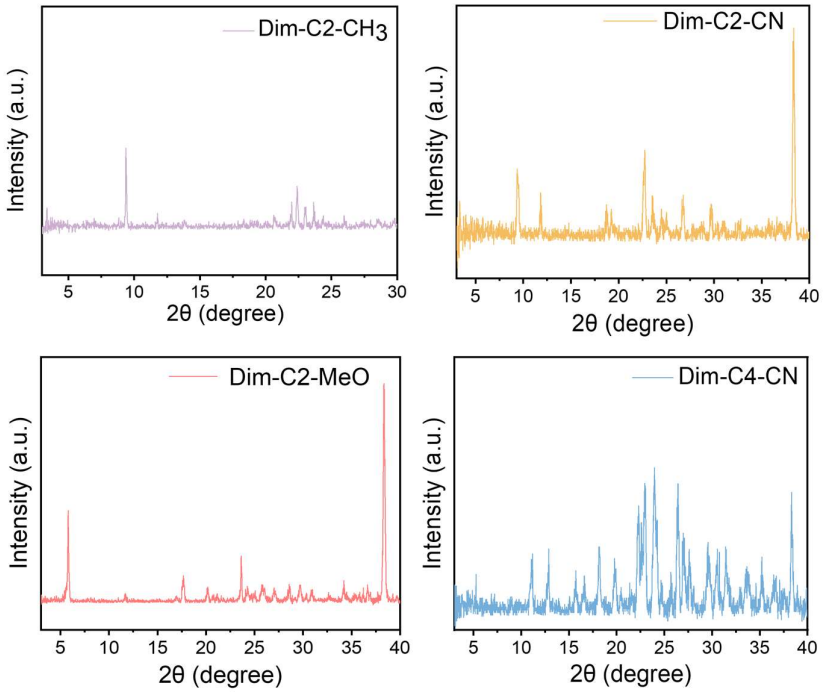

Fig. S15. XRD patterns of organic ligands: Dim-C2-CH_3, Dim-C2-CN, Dim-C2-MeO and Dim-C4-CN.

Action: (In page 4)

We synthesized high-quality single crystals through controlled co-crystallization of PbI_2 with each tailored ligand to validate the proposed low-dimensional perovskite. Optical microscopy and X-ray diffraction (XRD) analysis of organic ligands and single crystals confirmed high crystallinity across all four systems, with experimental patterns in excellent agreement with simulated diffractions (Supplementary Figs. S14-16). As predicted by DFT calculations, we obtained a 0D perovskite crystal (space group R-3, Supplementary Tables S1-8) using the Dim-C2-CH_3 ligand, formulated as (Dim-C2-CH_3)$_3$$Pb_3I_{4.9}Br_{7.1}$

3. Will the formation of 1d-3d hybrid perovskites affect the hydrophobicity of the film? It is recommended to provide contact Angle data.

Response: We appreciate the reviewer's thoughtful question. Contact angle measurements reveal that the reference perovskite film has a contact angle of 45°, which increases to 60° for the Dim-C4-CN-modified perovskite film. This increase demonstrates the superior hydrophobicity of the Dim-C4-CN-modified perovskite structure.

Action: (In the supporting information)

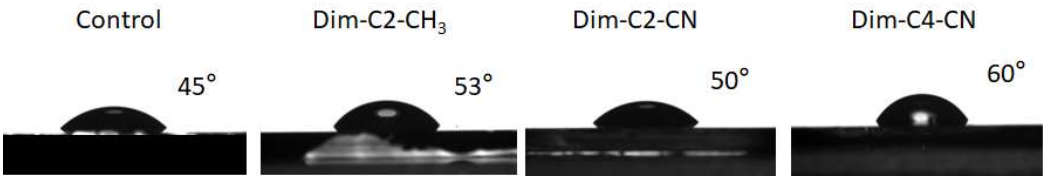

Fig.S55. Contact angle of perovskite films.

Action: (In page 10)

Among which, unencapsulated Dim-C4-CN-modified devices retained 90.8% of their initial efficiency after 5000 hours of storage at 40 ± 5% relative humidity (RH) and room temperature (ISOS-D-1), significantly outperforming the reference devices (43.9% retention under the same conditions) (Fig. 4d). The enhancement in humidity stability is attributed to the improved hydrophobicity (Figure S55) and the superior film quality. Furthermore, long-term operational stability was assessed under continuous

illumination (2000 hours, 60 °C, N_2 atmosphere, ISOS-L-2I), with the devices maintaining 94.3% of their initial efficiency (Fig. 4e).

4. Does the formation of low-dimensional perovskite change the residual strain in 3D perovskite films? It is suggested that the author provide evidence to illustrate. Please reference: https://doi.org/10.1002/aenm.202101018.

Response: We thank the reviewer for raising this question. To investigate the specific influence of low-dimensional perovskite on the stress within the 3D perovskite film, we have conducted Grazing-Incidence X-ray Diffraction (GIXRD) measurements with the sin2ψ method for both reference and Dim-C4-CN-modified perovskite films. In essence, perovskite film stress (σ) was determined by fitting 2θ as a function of $\sin^2\psi$, whereby the magnitude of residual strain was elucidated through the slope of the fitted line. Notably, the Dim-C4-CN-modified perovskite film displayed a markedly diminished negative slope compared to the control film, as indicated by the linear fit of $\sin^2\psi$ (Figure R4).

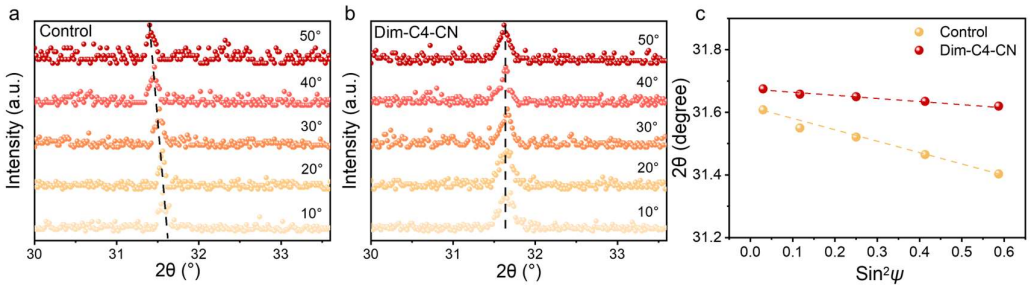

Figure R4. GIXRD patterns for both the (a) control and (b) Dim-C4-CN-modified perovskite films utilizing various instrumental ψ values ranging from 10 to 50°. (c) The linear fitting of 2θ-sin2ψ for both control and Dim-C4-CN-modified perovskite films.

Action: (In page 10)

The reduction in defect state density achieved through low-dimensional perovskite formation was further confirmed by space-charge-limited current (SCLC) measurements[35,36] (Supplementary Figs. S34-35), providing additional quantitative confirmation of the improved electronic quality in modified films. To probe the specific impact of low-dimensional perovskite on the strain state within the three-dimensional perovskite matrix, grazing-incidence X-ray diffraction (GIXRD) measurements coupled with the sin²ψ method were performed on both the reference and Dim-C4-CN-

modified perovskite films. Specifically, the film stress (σ) was determined by fitting the variation of 2θ as a function of $\sin^2\psi$, from which the extent of residual strain was inferred based on the slope of the linear regression. Remarkably, the Dim-C4-CN-modified perovskite film exhibited a substantially reduced negative slope relative to the control film, as evidenced by the linear fitting of $\sin^2\psi$ (Supplementary Figs. S36).

Action: (In the supporting information)

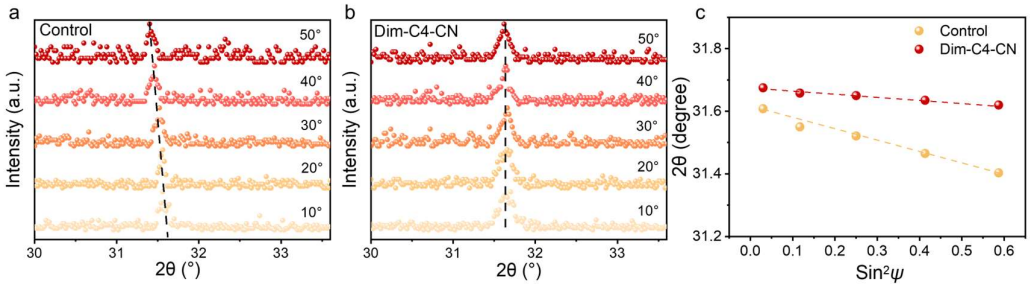

Fig. S36. GIXRD patterns for both the (a) control and (b) Dim-C4-CN-modified perovskite films utilizing various instrumental ψ values ranging from 10 to 50°. (c) The linear fitting of 2θ-sin2ψ for both control and Dim-C4-CN-modified perovskite films.

5. The author should further prove "Upon increasing the concentration of the three ligands, well-defined low-dimensional perovskite phases were preferentially accumulating at 3D perovskite grain boundaries" through experimental data.

Response: In response to the reviewer's suggestion, we provided SEM images of perovskite films treated with three different ligands at various concentrations. At a ligand concentration of 0.2 mg/mL, no obvious low-dimensional perovskite phases were observed in the SEM images for any of the three ligands. When the concentration was increased to 0.5 mg/mL, low-dimensional perovskites were predominantly distributed along the perovskite grain boundaries (Figure R5). To further investigate the distribution of low-dimensional phases at higher ligand concentrations, we acquired SEM images of perovskite films treated with Dim-C4-CN at concentrations of 0.3, 0.5, 0.75, and 1.0 mg/mL. With increasing concentration, a greater number of low-dimensional perovskite domains were observed at the grain boundaries, as highlighted by red circles in the images (Figure R6).

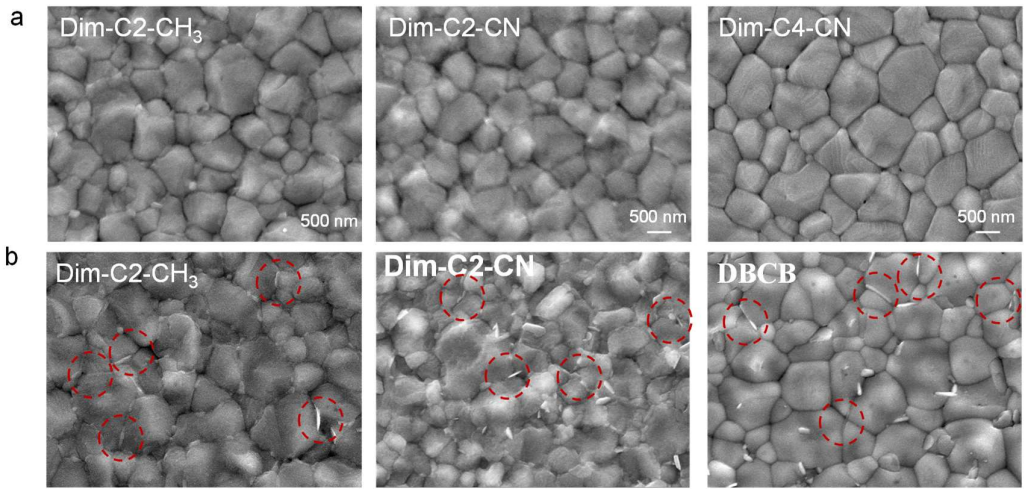

Figure R5. SEM images of perovskite films treated with organic ligands at concentrations of 0.2 mg/mL and 0.5 mg/mL.

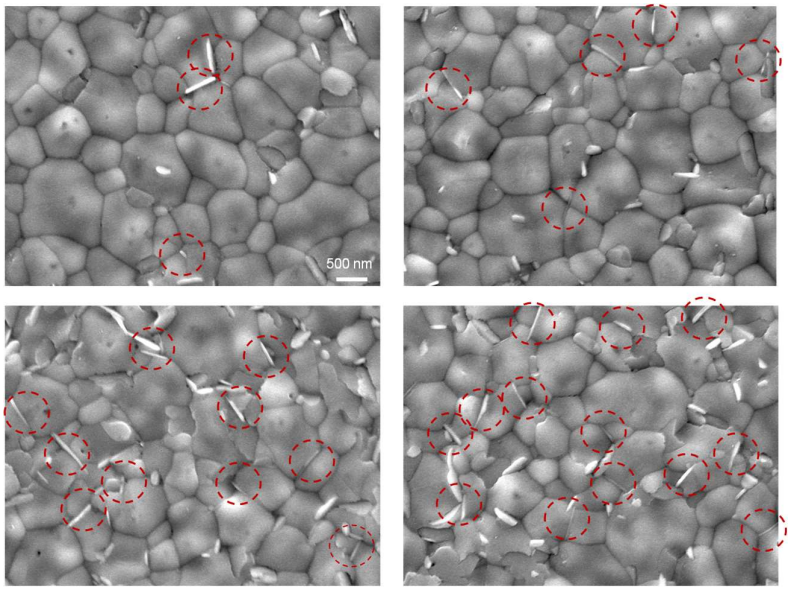

Figure R6. SEM images of perovskite films treated with Dim-C4-CN at concentrations of 0.3, 0.5, 0.75, and 1.0 mg/mL.

Action: (In page 10)

Systematic scanning electron microscopy (SEM) analysis revealed that Dim-C4-CN-modified perovskite films exhibited markedly improved morphological homogeneity and enhanced grain growth (Supplementary Figs. S21-22). Upon increasing the concentration of the three ligands, well-defined low-dimensional perovskite phases were preferentially accumulating at 3D perovskite grain boundaries (Supplementary Figs. S23-24). Atomic force microscopy (AFM) further corroborated these observations, revealing a substantial improvement in film quality following Dim-C4-CN

modification, as quantified by a reduction in surface roughness from 47.4 nm (unmodified reference film) to 21.2 nm (Dim-C4-CN-modified film) (Fig. 2a).

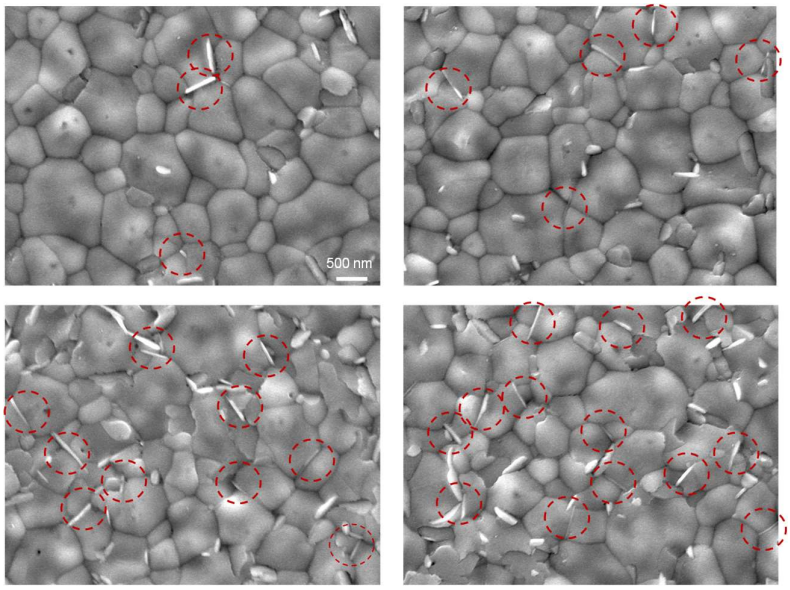

Fig. S24. SEM images of perovskite films treated with Dim-C4-CN at concentrations of 0.3, 0.5, 0.75, and 1.0 mg/mL.

6. The positions of the Pb 4f7/2 and Pb 4f5/2 peaks in Fig. S30 are incorrect. It is recommended that the author correct them.

Response: We thank the reviewer for highlighting this critical issue. In response, the positions of the Pb 4f7/2 and Pb 4f5/2 peaks have been corrected.

Action: (In the supporting information)

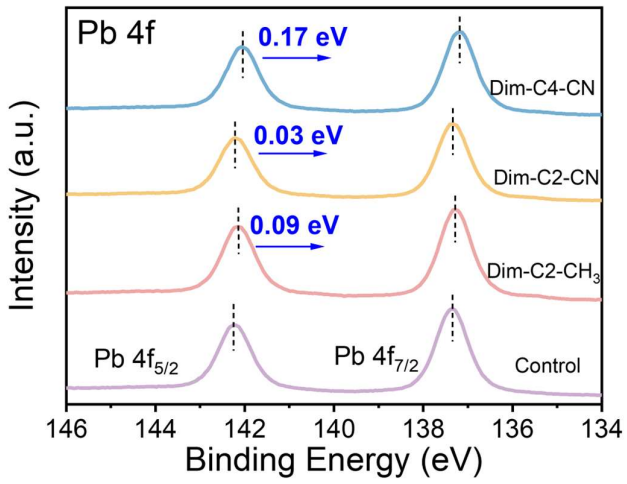

Fig. S32. XPS spectra of reference, Dim-C2-CH_3-, Dim-C2-CN-, and Dim-C4-CN-modified perovskite films.

7. It is suggested that the authors standardize the format of the nuclear magnetic resonance hydrogen spectra of the molecules in Figures S1-S8; it is recommended that the format of the relative energy values of molecules in Figures S9-S12 be unified.

Response: We sincerely appreciate the reviewers' thorough examination. Accordingly, we have standardized the format of the nuclear magnetic resonance hydrogen spectra of the molecules in Figures S1-S8; and the format of the relative energy values of molecules in Figures S9-S12 are also unified

Action: (In the supporting information)

[FIGURE REDACTED]

Fig. S2. ^{1}H NMR spectrum of Dim-C2-CH_3 molecule.

[FIGURE REDACTED]

Fig. S4. ^{1}H NMR spectrum of Dim-C2-CN molecule.

[FIGURE REDACTED]

Fig. S6. ^{1}H NMR spectrum of Dim-C4-CN molecule.

[FIGURE REDACTED]

Fig. S8. ^{1}H NMR spectrum of Dim-C2-OMe molecule.

Action: (In the supporting information)

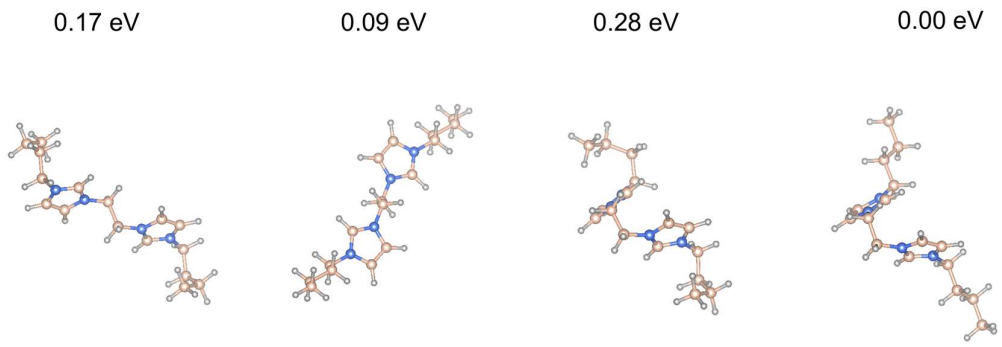

Fig. S9. Optimized molecular configurations of Dim-C2-CH_3 in DMSO with the relative energies, computed at the PBE0/cc-pVTZ level.

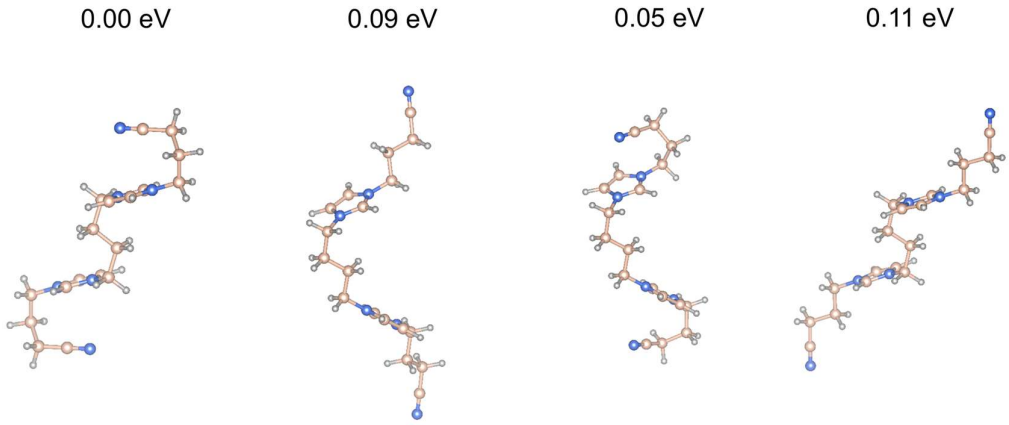

Fig. S12. Optimized molecular configurations of Dim-C4-CN in DMSO with the relative energies, computed at the PBE0/cc-pVTZ level.

8. "mofidied" in the caption of Fig. 2 should be "modified", and the spelling needs to be proofread.

Response: We thank the reviewer for the thorough examination. The manuscript has been carefully checked and all typographical errors have been corrected accordingly.

Action: (In page 23)

Fig. 2. Characterization of perovskite films. (**a**) AFM and (**c**) KPFM images of control, Dim-C2-CH_3, Dim-C2-CN and Dim-C4-CN-modified perovskite films. (**c**) Statistical analysis of potential distribution. (**d**) PL mapping of control, Dim-C2-CH_3, Dim-C2-CN and Dim-C4-CN-mofidied perovskite films.

Reviewer #3:

In this work, the authors successfully synthesized and characterized four distinct perovskite single-crystal structures by systematically modulating organic ligand chemistry. These crystals were effectively integrated into perovskite photovoltaic devices, achieving a certified power conversion efficiency (PCE) exceeding 27% along with excellent operational stability. The study demonstrates significant innovation, particularly in establishing explicit structure-property relationships between organic ligand design and low-dimensional crystal architectures. Supported by comprehensive characterization, I believe this work will significantly advance future research on low-dimensional/three-dimensional (2D/3D) heterojunction systems. Therefore, I would recommend this manuscript for publication in Nature Communications after the following revisions are addressed.

Response: We thank the reviewer for the positive comments.

1.Regarding the single-crystal structures induced by the Dim-C2-CN and Dim-C4-CN ligands, does the current study focus exclusively on cyano (-CN) modified systems? It would be helpful to know if the investigation was extended to explore the specific crystal structures induced by ligands functionalized with other types of substituents, or if the -CN group was specifically chosen for a particular chemical reason.

Response: We sincerely appreciate the reviewer's insightful question. In our study, the investigation was not limited to cyano (-CN) modified ligands. For the single-crystal structure induced by the Dim-C2-CN ligand, DFT calculations revealed that replacing the -CN group with $-CH_3$ or -OH leads to formation energies of -5.35 eV and -5.63 eV, respectively, which are lower than that of the cyano-containing system (Figure R2). Similarly, in the analysis of the single-crystal structure induced by Dim-C4-CN, DFT calculations showed that substituting the -CN group with $-CH_3$ (-6.28 eV) or -OH (-6.43 eV) also reduces the crystal formation energy compared to that of the -CN system (-6.71 eV) (Figure R3).

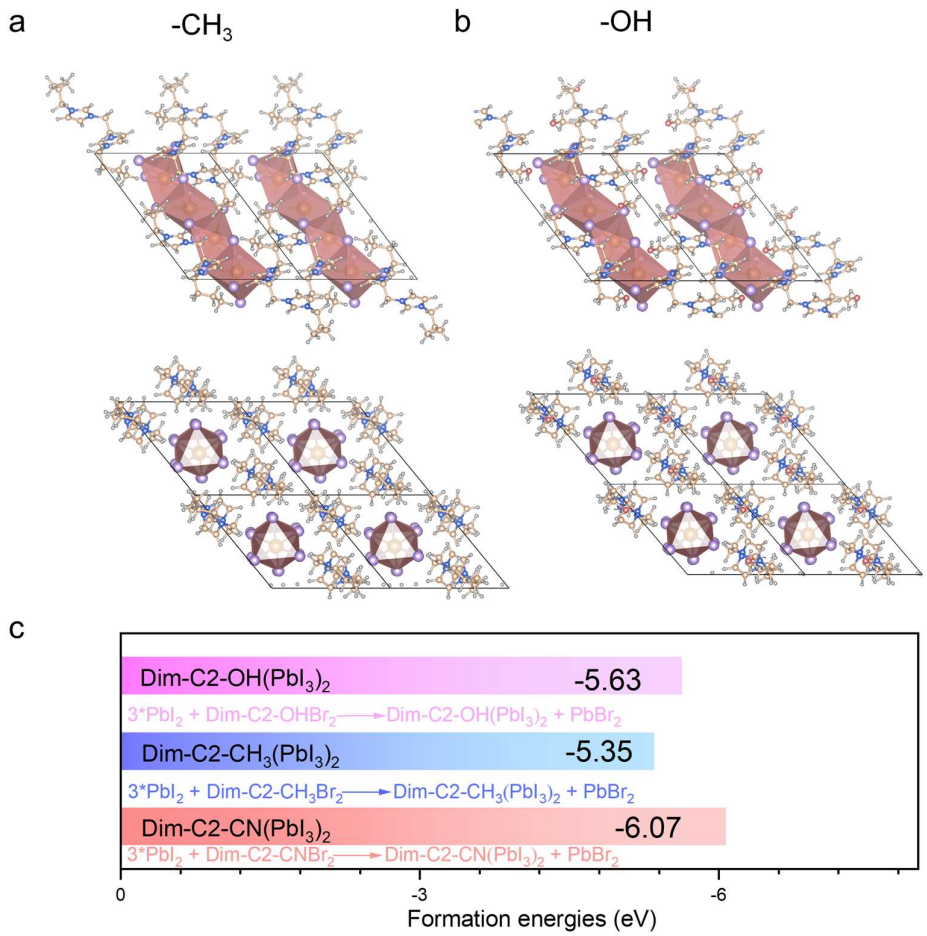

Figure R2. Side (first row) and top view (second row) of the DFT optimized crystal structures of (a) Dim-C2-$CH_3(PbI_3)_2$ and (b) Dim-C_2-$OH(PbI_3)_2$. (c) Formation energies of the Dim-C2-$CH_3(PbI_3)_2$, Dim-C2-$CH_3(PbI_3)_2$, and Dim-C2-$CH_3(PbI_3)_2$ crystals computed by DFT calculations.

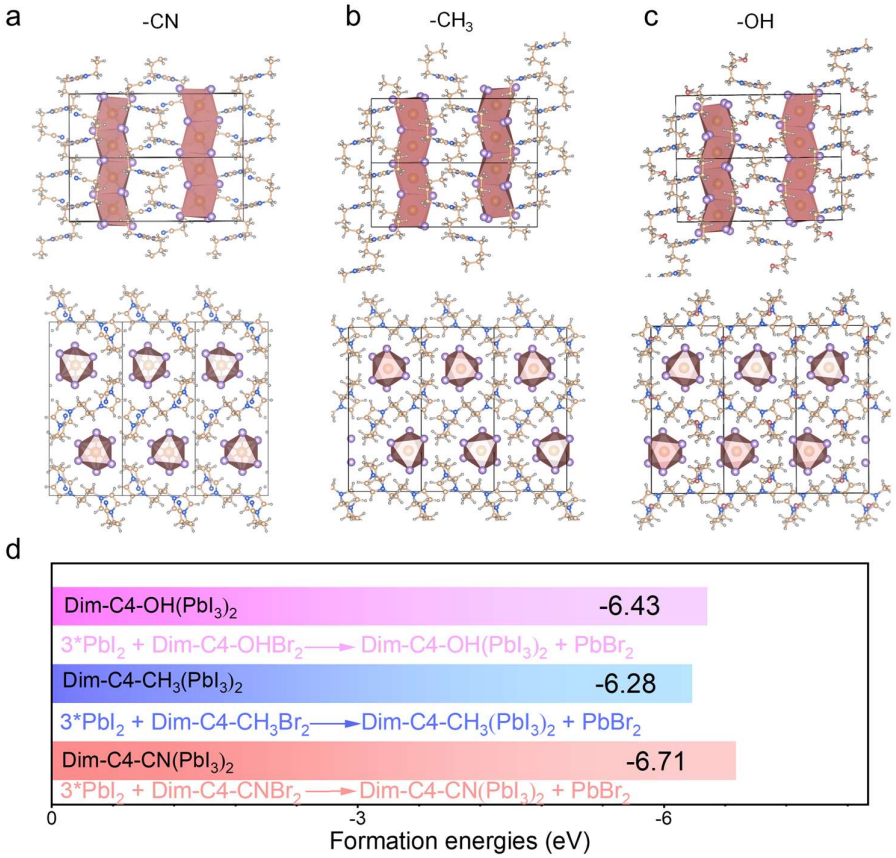

Figure R3. (a-c) Simulation of the single crystal structure 1D Dim-C4-CN$(PbI_3)_2$ after replacing the -CN in the ligand Dim-C4-CN with a -CH_3 or -OH group. Formation energies of the Dim-C4-$CH_3(PbI_3)_2$, (Dim-C4-$CH_3(PbI_3)_2$, and Dim-C4-$CH_3(PbI_3)_2$ crystals computed by DFT calculations.

Action: (In page 5)

The ligands with methoxy groups (Dim-C2-OMe) and cyano groups (Dim-C2-CN) both yield a 1D perovskite crystal Dim-C2-OMe$(PbI_3)_2$ (Supplementary Tables S9-16) and Dim-C2-CN$(PbI_3)_2$ (Supplementary Tables S17-24), where the terminal distances reduced to 4.90 and 4.06 Å (Fig. 1c), respectively in line with the DFT results. Moreover, the DFT calculations show an isostructural 1D perovskite crystal when replacing the CN groups with OH groups (Supplementary Figs. S17-18) and the CN groups (-6.07 eV) showed larger crystal formation energy than the CH_3 (-5.35 eV) and OH (-5.63 eV) groups.

Action: (In page 5)

Extending inter-imidazolium chain length from Dim-C2-CN scaffold to Dim-C4-CN transformed the parallel 1D orientation to a bridged 1D architecture (Fig. 1d), Dim-C4-

$CN(PbI_3)_2$, which is classified within the monoclinic crystal (space group P 21/c. Supplementary Tables S25-31). This configuration enhances interchain connectivity via ligand-mediated bridging, markedly stabilizing the perovskite framework. DFT calculations show that further substitution of CN groups (-6.71 eV) with CH_3 (-6.28 eV) or -OH (-6.43 eV) groups reduced the crystal formation energy(Supplementary Figs. S19-20). The formation energy of Dim-C4-CN $(PbI_3)_2$ (-6.71 eV) is lower than that of Dim-C2-CN $(PbI_3)_2$ (-6.07 eV), indicating stronger thermodynamic stability of the Dim-C4-CN-induced 1D perovskite structure.

2.When substituting a methyl group with a cyano group on the ligand, it is necessary to elucidate the specific advantages conferred by this modification, either in terms of the ligand's own properties or the resulting single-crystal packing. Please provide a clearer rationale for the selection of CN-functionalized ligands in this study.

Response: Regarding the selection of the cyano group over the methyl group on the ligand, our decision was primarily driven by the high polarity and strong coordination capability of the cyano functionality. These properties enable it to engage in coordination interactions with lead ions (Pb^{2+}) in perovskite precursors. Such interactions effectively modulate the crystallization kinetics, thereby facilitating the formation of dense and morphologically uniform thin films. Furthermore, the cyano group plays a critical role in suppressing ion migration within the perovskite lattice and contributes to efficient defect passivation by bonding with defect sites, as supported by recent literature (Nature 2024, 628, 306–312; Nat. Mater. 2025, 24, 770–777; Angew. Chem. Int. Ed. 2025, 64, e202504902).

In this study, we employed in situ grazing-incidence wide-angle X-ray scattering (GIWAXS) and in situ absorption spectroscopy to validate the role of the cyano-containing ligand Dim-C4-CN in regulating the perovskite crystallization process. Analysis of the GIWAXS patterns further indicated that Dim-C4-CN promotes the formation of perovskite thin films with enhanced crystallinity.

Additionally, to compare the single-crystal structures induced by cyano- and methyl-modified ligands, we performed DFT calculations to determine the formation

energies in the Dim-C2-CN and Dim-C4-CN systems. The results revealed that the formation energies of single crystals induced by cyano-functionalized ligands are consistently higher than those induced by their methyl-substituted counterparts, providing energetic evidence for the role of the cyano group in stabilizing the crystal lattice.

Action: (In page 8)

Furthermore, in-situ GIWAXS analysis was also conducted on Dim-C2-CH_3-modified perovskite thin films (Supplementary Fig. S38). Unlike the rapid crystallization observed in 1D perovskites, the formation of 0D perovskite structures necessitates extended annealing durations, which can be ascribed to pronounced interaction between the Dim-C4-CN ligand and the perovskite constituents, coupled with their inherently lower formation energy. These transient 1D perovskite phase perform two critical functions: (i) they kinetically compete with and retard the direct reaction between PbI_2 and organic salts and (ii) they serve as structural templates to guide the oriented growth of 3D perovskite domains. This dual functionality establishes a more a more effective pathway for crystallization control, enabling the formation of high-quality perovskite films with improved morphological and electronic preperties[39].

Action: (In page 5)

The ligands with methoxy groups (Dim-C2-OMe) and cyano groups (Dim-C2-CN) both yield a 1D perovskite crystal Dim-C2-OMe$(PbI_3)_2$ (Supplementary Tables S9-16) and Dim-C2-CN$(PbI_3)_2$ (Supplementary Tables S17-24), where the terminal distances reduced to 4.90 and 4.06 Å (Fig. 1c), respectively in line with the DFT results. Moreover, the DFT calculations show an isostructural 1D perovskite crystal when replacing the CN groups with OH groups (Supplementary Figs. S17-18) and the CN groups (-6.07 eV) showed larger crystal formation energy than the CH_3 (-5.35 eV) and OH (-5.63 eV) groups.

Action: (In page 5)

Extending inter-imidazolium chain length from Dim-C2-CN scaffold to Dim-C4-CN transformed the parallel 1D orientation to a bridged 1D architecture (Fig. 1d), Dim-C4-

$CN(PbI_3)_2$, which is classified within the monoclinic crystal (space group P 21/c. Supplementary Tables S25-31). This configuration enhances interchain connectivity via ligand-mediated bridging, markedly stabilizing the perovskite framework. DFT calculations show that further substitution of CN groups (-6.71 eV) with CH_3 (-6.28 eV) or -OH (-6.43 eV) groups reduced the crystal formation energy(Supplementary Figs. S19-20). The formation energy of Dim-C4-CN $(PbI_3)_2$ (-6.71 eV) is lower than that of Dim-C2-CN $(PbI_3)_2$ (-6.07 eV), indicating stronger thermodynamic stability of the Dim-C4-CN-induced 1D perovskite structure.

3.The origin of the simplified structural representation in Figure 1c should be clarified. Please specify whether it was obtained through computational simulation (e.g., DFT) or if it is a schematic abstraction of an experimentally determined single-crystal structure.

Response: We thank the reviewer for the suggestion. A source note for Figure 1c has been added to the corresponding figure caption to clarify its origin.

Action: (In page 22)

Fig. 1. Ligands and the corresponding single-crystal structures. (**a**) The chemical structure of the ligand. (**b**) The optimized ball-and-stick model of the ligand. (**c**) Simplified single-crystal structure diagram is derived from the single-crystal structure data. (**d**) The single-crystal structural characteristics of low-dimensional perovskites induced by four distinct ligands. (**e**) The ligand molecular structure and perovskite dimensional selectivity correlation model.

4.For the stability tests conducted under 85°C and 85% relative humidity (ISOS-D-3), the authors should present the actual efficiency evolution data (absolute PCE values) in the supplement, rather than reporting only the normalized efficiency values.

Response: We thank the reviewer for the valuable suggestion. Accordingly, we have included an additional plot showing the evolution of the actual efficiency over time during the stability test.

Action: (In the supporting information)

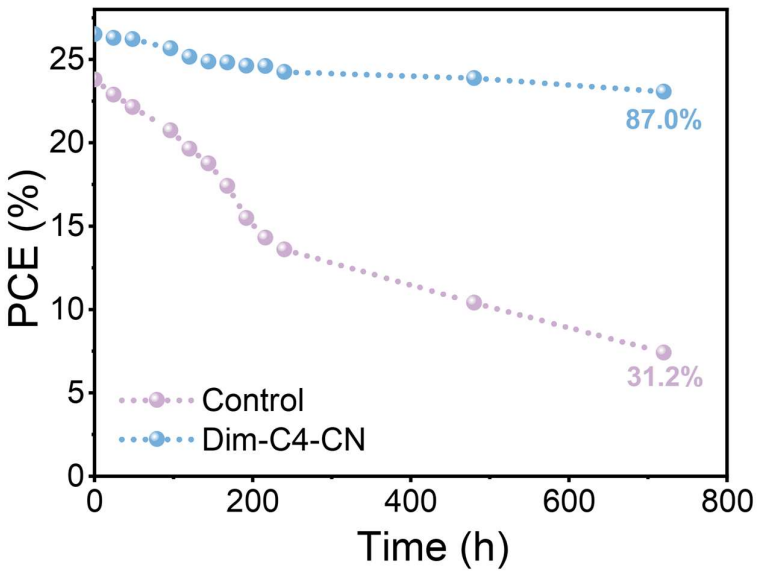

Figure S56. Long-term stability of control and Dim-C4-CN-modified devices monitoring at 85% RH and 85 °C (ISOS-D-3).

Action: (In page 10)

Furthermore, long-term operational stability was assessed under continuous illumination (2000 hours, 60 °C, N_2 atmosphere, ISOS-L-2I), with the devices maintaining 94.3% of their initial efficiency (Fig. 4e). Long-term stability monitoring at 85% RH and 85 °C (ISOS-D-3) revealed that the Dim-C4-CN-modified devices retained 87% of their initial PCE after 800 hours of continuous operation (Supplementary Fig. S56).

5.It was observed that the optimal concentrations of the added ligands differ between the 1.54 eV and wide-bandgap (WBG) devices. To better understand these system-dependent effects, the impact of varying ligand concentrations on device performance should be systematically discussed across the different bandgap regimes.

Response: We thank the reviewer for the helpful suggestion. In response, we conducted a detailed optimization of the ligand concentration in perovskite systems with bandgaps of 1.67 eV and 1.84 eV, and have included the corresponding photovoltaic parameters of the devices in the Supporting Information.

Action: (In page 9)

Based on the aforementioned 1D modification strategy, devices with an effective area of 1 cm^2 were fabricated, achieving an optimal efficiency of 25.95% (Supplementary

Figs. S50). The implementation of this dimensional strategy enabled the successful scaling of perovskite photovoltaics to 30×30 cm^2 perovskite solar modules, resulting in a champion PCE of 21.41% (Fig. 4c). Notably, our approach was also successfully extended to wide-bandgap perovskite, including 1.67-eV (Supplementary Fig. S51-52 and Supplementary Table S36) and 1.84-eV (Supplementary Fig. S53-54 and Supplementary Table S37) bandgap perovskite solar cells, where the Dim-C4-CN-modified devices achieved a champion PCE of 23.45% and 19.00%, respectively, representing the universality and potential application value of the Dim-C4-CN.

Action: (In the supporting information)

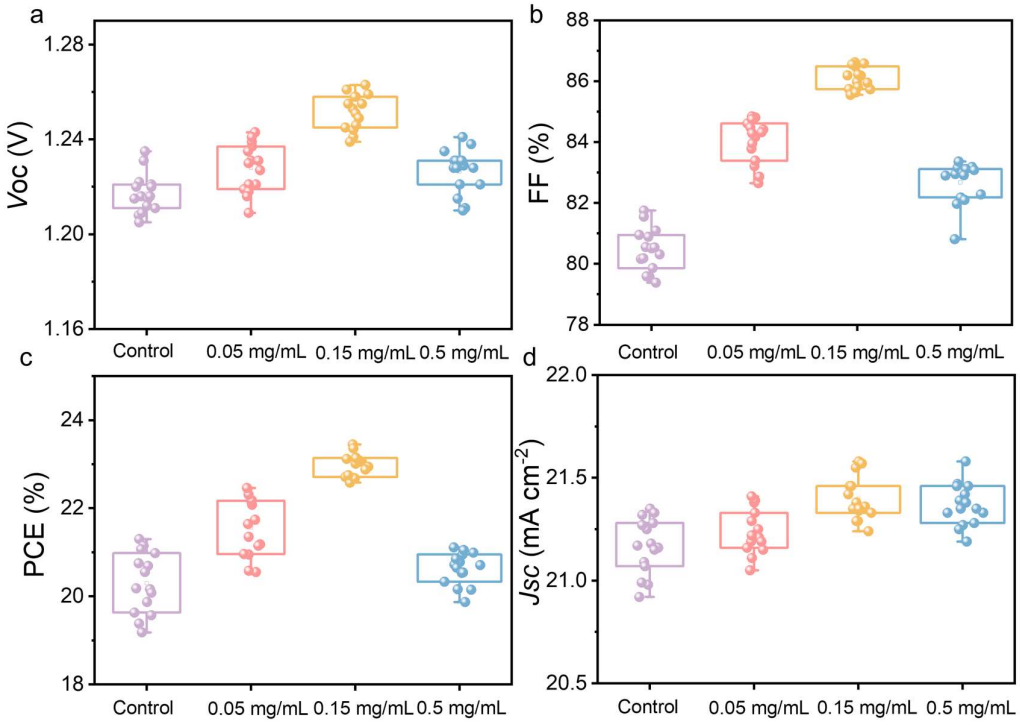

Fig. S52. Photovoltaic performance statistics of the devices with bandgaps of 1.67 eV treated with varying concentrations of Dim-C4-CN. The statistics of photovoltaic performance parameters of control and ligands-modified PSCs: (a) *V*oc, (b) FF, (c) PCE and (d) *J*sc.

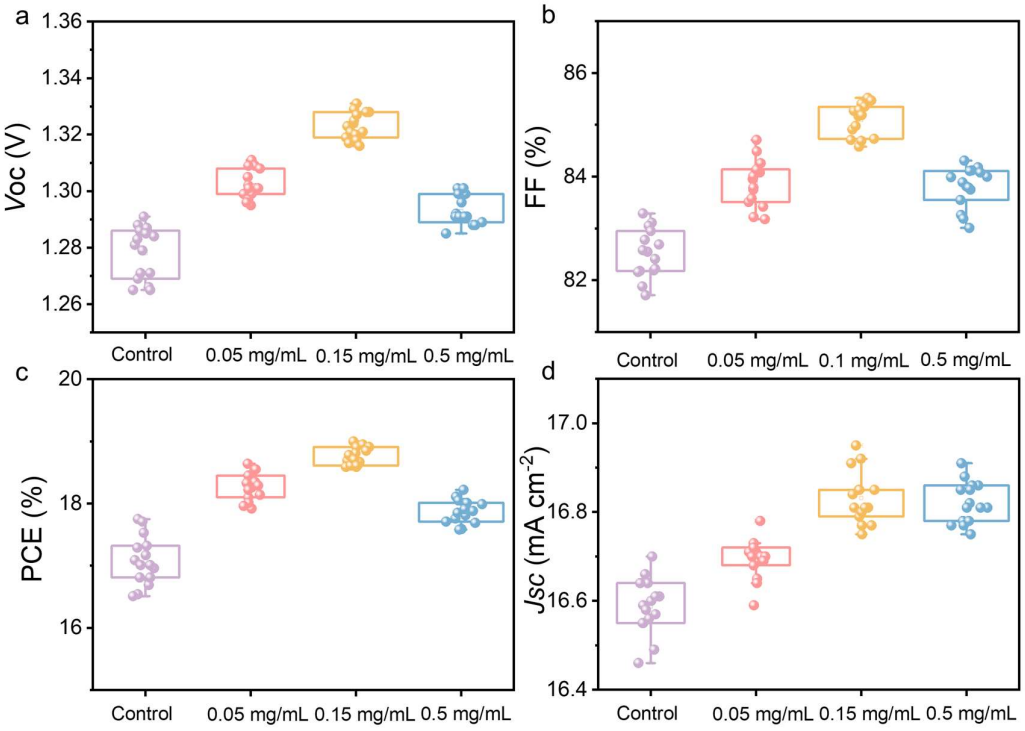

Fig. S54. Photovoltaic performance statistics of the devices with bandgaps of 1.84 eV treated with varying concentrations of Dim-C4-CN. The statistics of photovoltaic performance parameters of control and ligands-modified PSCs: (a) *V*oc, (b) FF, (c) PCE and (d) *J*sc.

6.There appears to be an inaccuracy in the caption of Figure 2. The authors should carefully verify and correct the descriptions to ensure they match the data shown.

Response: We thank the reviewer for the thorough examination. The manuscript has been carefully checked and all typographical errors have been corrected accordingly.

Action: (In page 23)

Fig. 2. Characterization of perovskite films. (**a**) AFM and (**c**) KPFM images of control, Dim-C2-CH_3, Dim-C2-CN and Dim-C4-CN-modified perovskite films. (**c**) Statistical analysis of potential distribution. (**d**) PL mapping of control, Dim-C2-CH_3, Dim-C2-CN and Dim-C4-CN-mofidied perovskite films.